Bidirectional dysregulation of synaptic glutamate signaling after transient metabolic failure

Stefan Passlick [1], Ghanim Ullah [2], Christian Henneberger [1, 3, *]

1 Institute of Cellular Neurosciences, Medical Faculty, University of Bonn, Bonn, Germany

2 Department of Physics, University of South Florida, Tampa, FL 33620, USA

3 German Center for Neurodegenerative Diseases, Bonn, Germany

* Corresponding author (christian.henneberger@uni-bonn.de)

Abstract

Ischemia leads to a severe dysregulation of glutamate homeostasis and excitotoxic cell damage in the brain. Shorter episodes of energy depletion, for instance during peri-infarct depolarizations, can also acutely perturb glutamate signaling. It is less clear if such episodes of metabolic failure also have persistent effects on glutamate signaling and how the relevant mechanisms such as glutamate release and uptake are differentially affected. We modelled acute and transient metabolic failure by using a chemical ischemia protocol and analyzed its effect on glutamatergic synaptic transmission and extracellular glutamate signals by electrophysiology and multiphoton imaging, respectively, in the hippocampus. Our experiments uncover a duration-dependent bidirectional dysregulation of glutamate signaling. Whereas short chemical ischemia induces a lasting potentiation of presynaptic glutamate release and synaptic transmission, longer episodes result in a persistent postsynaptic failure of synaptic transmission. We also observed unexpected differences in the vulnerability of the investigated cellular mechanisms. Axonal action potential firing and glutamate uptake were unexpectedly resilient compared to postsynaptic cells, which overall were most vulnerable to acute and transient metabolic stress. We conclude that even short perturbations of energy supply lead to a lasting potentiation of synaptic glutamate release, which may increase glutamate excitotoxicity well beyond the metabolic incident.

Introduction

It is well established that the breakdown of ATP production in the brain in an ischemic stroke, profoundly affects glutamate signaling on various levels. The inability of neurons and other cell types such as astrocytes to maintain transmembrane ionic gradients and their membrane

potential leads to increased glutamate release, decreased glutamate clearance, and, thereby, increased glutamate receptor activation and excitotoxicity, which ultimately results in cell death (Dirnagl et al., 1999). The ischemic core is also the source of peri-infarct depolarizations that travel into the primarily undamaged tissue. They are a relatively short-lasting sub-type of spreading depolarizations associated with a significant metabolic burden that can lead to the progressive expansion of tissue damage in the peri-infarct zone (Lauritzen et al., 2011). In animal models of ischemic stroke, they can be detected as transient glutamate increases lasting about a minute using for instance microdialysis and fluorescence imaging (Lauritzen et al., 2011; Rakers and Petzold, 2017). In addition to neuronal glutamate release, glial glutamate release and a transient reduction of glutamate uptake could contribute to such transient glutamate increases (Lauritzen et al., 2011; Rakers and Petzold, 2017; Passlick et al., 2021). Whether peri-infarct depolarizations, and spreading depolarizations in general, acutely trigger lasting changes of glutamate signaling and homeostasis is far less clear.

Spreading depression is accompanied by a transient decrease of ATP levels (Mies and Paschen, 1984). This decrease can be reproduced in vitro by creating anoxic conditions, removal of substrates for ATP production such as glucose, inhibition of metabolic pathways, or combinations of these manipulations. In vitro studies using such approaches to induce a transient metabolic failure have demonstrated for instance that brief periods of anoxia and aglycemia lead to a persistent potentiation of synaptic transmission at CA3-CA1 synapses in the hippocampus, also called ischemic or anoxic long-term potentiation (LTP) (Crepel et al., 1993, 2003; Hsu and Huang, 1997; Stein et al., 2015). This indicates that a transient metabolic failure can persistently alter glutamatergic synaptic transmission. Whether this also applies to glutamate release and glutamate uptake is currently not known but potentially important, because that may increase the likelihood of increased excitability and excitotoxicity in between individual peri-infarct depolarizations.

For these reasons, we explored if and how short and transient periods of metabolic failure affect glutamate release and uptake in parallel to synaptic transmission using combinations of electrophysiology and glutamate imaging in the hippocampus together with a chemical ischemia protocol. We observed a duration-dependent bidirectional dysregulation of glutamate release and synaptic transmission, in which short durations of chemical ischemia led to a persistent potentiation of glutamate release while long durations induced postsynaptic failure. We further uncovered unexpected differences of vulnerability of mechanisms involved in glutamatergic synaptic transmission, including a marked resilience of glutamate uptake to chemical ischemia.

Results

Bidirectional dysregulation of glutamate signaling

For revealing the effect of acute and transient metabolic failure on glutamatergic synaptic transmission, we combined electrophysiological monitoring of glutamatergic synaptic transmission at CA3-CA1 Schaffer collateral synapses in acute hippocampal slices with a chemical ischemia model. Baseline synaptic transmission was monitored for >10 minutes before ATP production was disrupted by switching to a modified extracellular solution lacking glucose and containing sodium azide and 2-deoxyglucose to inhibit oxidative phosphorylation and glycolysis, respectively (schematic in **Fig. 1A**). This protocol for 'chemical ischemia' has previously been shown to reliably induce a rapid and reversible decline of the intracellular ATP levels (Pape and Rose, 2023). We first tested the effect of acute and transient chemical ischemia lasting for 2 to 5 minutes and observed two qualitatively distinct results. A comparison of recordings with 2 and 5 minutes illustrates both scenarios (**Fig. 1B-F**). Although the postsynaptic response transiently disappeared for both durations, they remained suppressed over the next 50 minutes of recording for 5 min of chemical ischemia but recovered when chemical ischemia lasted only 2 minutes, in which case it showed a significant potentiation at the end of the recording (**Fig. 1B, C, E**). In contrast, the axonal fiber volley, which reflects the axonal firing of action potentials after stimulation, was transiently suppressed and recovered fully for both durations (**Fig. 1D**). Analyzing the entire data set including chemical stress durations of 3 and 4 minutes confirmed that the axonal fiber volley robustly recovered from chemical ischemia for the tested duration (**Fig. 1G**). In contrast, the postsynaptic response was either potentiated for shorter durations or almost completely suppressed for longer durations (**Fig. 1H**). For chemical ischemia with near complete suppression of the postsynaptic response (**Fig. 1H**, orange data points), the average duration of chemical stress was 4.46 ± 0.207 minutes (n = 11) and 2.74 ± 0.20 minutes (n = 19) for all other recordings. Because the cellular depolarization and ensuing increased neuronal synaptic glutamate release should lead to an extracellular potassium increase, we measured extracellular [K^+] in parallel in a subset of experiments (example in **Fig. 1F**). Correlating the maximum increase of the extracellular [K^+] during chemical ischemia revealed that a stronger extracellular [K^+] increase (i.e., a severe metabolic failure) made postsynaptic failure more likely (**Fig. 1I**). Together, these experiments reveal two distinct outcomes of acute chemical ischemia: Either potentiation of the synaptic response or its near-complete suppression, which represents a postsynaptic failure of synaptic transmission as revealed by the following glutamate imaging experiments.

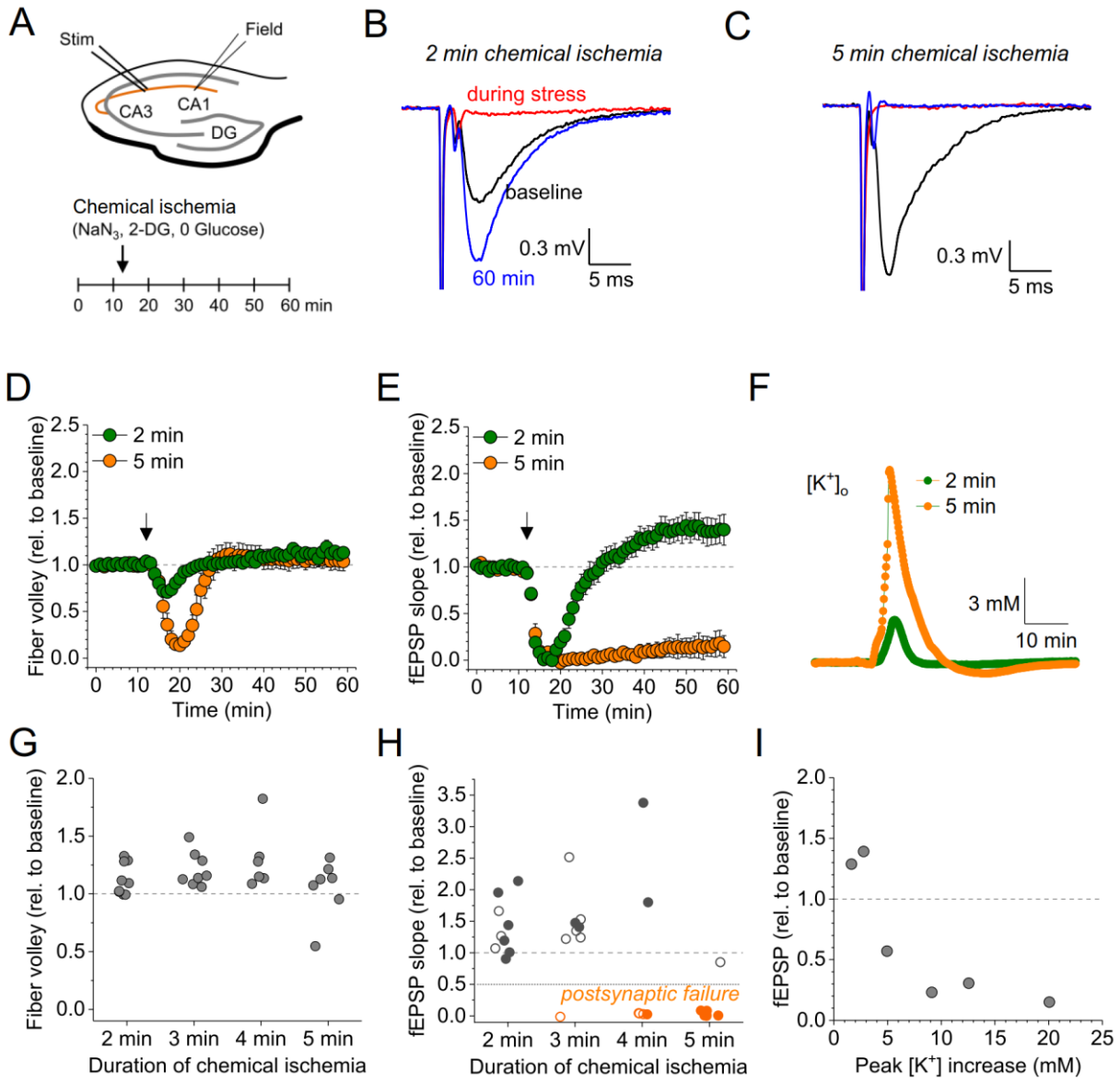

Figure 1: Duration-dependent and bidirectional effect of transient chemical ischemia on synaptic transmission. (A) Schematic of experimental design. Extracellular field potentials (Field) were recorded in the CA1 region in response to Schaffer collateral stimulation (Stim; paired pulses, 50 ms interstimulus interval, every 20 s). Arrow indicates the time point of application of a modified ACSF, inducing acute chemical ischemia, with 0 mM glucose, 2 mM deoxyglucose (2-DG), 5 mM sodium azide (NaN_3) for 2-5 min. (B-C) Example traces for 2 min chemical ischemia (B) and 5 min chemical ischemia (C) (black, baseline; red, during stress; blue, end of the experiment at 60 min). (D) Relative change of the axonal fiber volley amplitude compared to baseline (0-10 min) for 2 min of chemical ischemia (green) and 5 min of chemical ischemia (orange). Arrow indicates time point of application of the modified ACSF for chemical ischemia induction. (E) Same as in (D) but for the fEPSP slope. (F) Example traces of extracellular $[K^+]$ recordings during for 2 and 5 min of chemical ischemia. (G) Quantification of the relative change of the axonal fiber volley amplitude in the last 10 min of recordings (50-60 min) relative to baseline for 2, 3, 4 and 5 min (n = 9, 8, 6, and 7, respectively) of chemical ischemia. (H) Same experiments as in (G) but analysis of the fEPSP slope. Graphs in H and G include results from recording shown in B-E. Persistent failure of synaptic transmission highlighted

in orange. Filled circles correspond to recordings, in which astrocytes expressed iGluSnFR (see **Fig. 2** and text). (I) Change of fEPSP in the last 10 min of recordings (50-60 min) relative to the baseline plotted against maximum [K^+] increase during chemical ischemia. Data are expressed as mean ± s.e.m.

In a subset of the recordings shown in **Fig. 1H** (filled data points), we have combined electrophysiological recordings with monitoring of glutamate release using the fluorescent indicator iGluSnFR (Marvin et al., 2013) (**Fig. 2**). In this subset, iGluSnFR was virally expressed in astrocytes and its fluorescence changes were monitored in response to paired stimuli of CA3-CA1 synapses by line-scanning throughout the experiment as indicated in **Fig. 2A**-**B**. Additional control experiments confirmed the stability of such combined recordings (**Fig. 2C, F**). We grouped recordings combining iGluSnFR imaging and electrophysiology according to the effect of chemical ischemia on the synaptic response: 'chemical ischemia with postsynaptic failure' (**Fig. 1H**, filled orange data points) if the postsynaptic response did not recover to above 50% of the baseline level and 'chemical ischemia' when it did (**Fig. 1H**, filled dark grey data points). Similar to electrophysiological recordings, two response types could be identified in iGluSnFR recordings. When acute and transient chemical ischemia led to a persistent potentiation of synaptic transmission, this was associated with an increase of the iGluSnFR responses ($\Delta F/F_0$) (**Fig. 2D**). In contrast, if chemical ischemia led to postsynaptic failure, we observed a transient surge of the resting fluorescence of iGluSnFR (F_0) during acute chemical ischemia and reduced and gradually recovering iGluSnFR transients in response to synaptic stimulation after chemical ischemia (**Fig. 2E**). Presented are six out of the nine experiments with postsynaptic failure that were performed. Three recordings were not further analyzed because the iGluSnFR fluorescence became undetectable after chemical ischemia. A more comprehensive statistical analysis of the responses before and after chemical ischemia can be found in **Fig. S1** and **Fig. 2F, G, H**. In a single experiment, we have been able to record the response to two subsequent periods of short chemical ischemia in a > 3-hour recording (**Fig. S2**), which highlights the persistence of the potentiation of both the postsynaptic responses and glutamate transients. In addition to the bidirectional changes of synaptic transmission and glutamate release depending on the severity of chemical ischemia, we also found a consistent decrease of the iGluSnFR resting fluorescence over the duration of the experiments in all conditions. In general, this could be caused by a gradual reduction of the resting extracellular glutamate levels and/or a reduction of fluorescent iGluSnFR, for instance due to bleaching, which appears to be a likely explanation given the repeated imaging over up to 90 minutes. It is important to note that the increase of the iGluSnFR transients ($\Delta F/F_0$) associated with potentiated postsynaptic responses is unlikely due to the reduction of F_0 because the latter is observed in all

experimental conditions. Similarly, it is unlikely that the increase of the iGluSnFR transients is because of the increased axonal excitability (increased fiber volley amplitude) because this was also observed in control recordings, where no change of the iGluSnFR response ($\Delta F/F_0$) was detected. The increase of the iGluSnFR response after synaptic activation also points to an increase of extracellular glutamate transients, because the iGluSnFR response to saturating glutamate is unaffected in experiments with chemical ischemia without postsynaptic failure (**Fig. S3**).

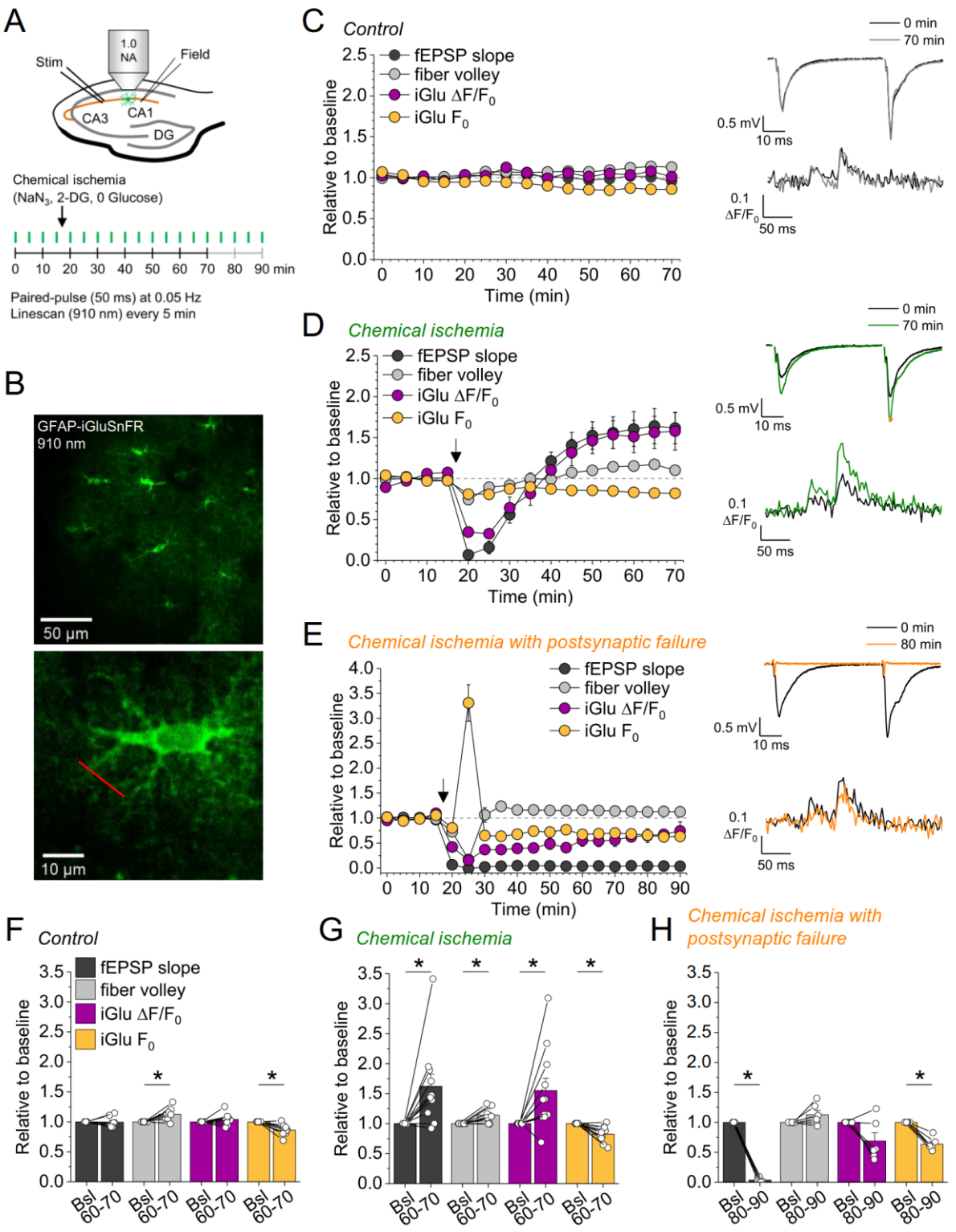

Figure 2: Bidirectional dysregulation of glutamate release by transient chemical ischemia. (A) Schematic of experimental design. Combined recording of extracellular field potentials (Field) in the CA1 region in response to Schaffer collateral stimulation (Stim; paired pulses, interstimulus interval of 50 ms, every 20 s) and two-photon excitation fluorescence line scan imaging (910 nm, 6x every 5 min) of the glutamate indicator iGluSnFR. (B) Top: example of virally induced GFAP-iGluSnFR expression by astrocytes in the *stratum radiatum* of the CA1 region. Bottom: single iGluSnFR-expressing astrocyte and representative location of line scan (red line). (C-E) Left, field excitatory postsynaptic

172 potential (fEPSP) slope, axonal fiber volley, iGluSnFR (iGlu) $\Delta F/F_0$ and iGlu resting fluorescence (F_0)
173 relative to baseline (0-10 min) for control (n = 8) (C), chemical ischemia (n = 11) (D) and chemical
174 ischemia followed by postsynaptic failure of synaptic transmission (n = 6) (E). Arrow indicates start of
175 chemical ischemia. Right, example traces of fEPSP (top) and iGluSnFR $\Delta F/F_0$ (bottom, average of 6
176 scans) at the beginning and the end of the recording. The electrophysiological results in D and E are a
177 subset from Fig. 1. (F-H) Summary of parameters analyzed in C-E in the last 10 min of recording (60-
178 70/80-90 min) compared to baseline (Bsl). (F) Control: fEPSP slope, $p = 0.894$; fiber volley, $p = 0.012$;
179 iGlu $\Delta F/F_0$, $p = 0.310$; iGlu F_0, $p = 0.006$; n = 8, paired Student's t-test. (G) Chemical ischemia: fEPSP
180 slope, $p = 0.013$; fiber volley, $p = 0.003$; iGlu $\Delta F/F_0$, $p = 0.024$; iGlu F_0, $p = 0.001$; n = 11, paired
181 Student's t-test. (H) Chemical ischemia with postsynaptic failure: fEPSP slope, $p < 0.0001$; fiber volley,
182 $p = 0.134$; iGlu $\Delta F/F_0$, $p = 0.073$; iGlu F_0, $p = 0.0004$; n = 6, paired Student's t-test. Data are expressed
183 as mean ± s.e.m.

184

185 Taken together these experiments reveal that longer durations of chemical ischemia result in
186 a persistent postsynaptic failure with slowly recovering glutamate release. A likely reason for
187 the postsynaptic failure is the death or persistent depolarization of CA1 pyramidal cells.
188 Although not quantified, we indeed observed irreversible swelling and/or loss of integrity of
189 CA1 pyramidal cell bodies in parallel to postsynaptic failure. This is in line with previous
190 studies using transient metabolic inhibition with similar durations, which reported irreversible
191 ATP depletion in neocortical neurons after transient chemical ischemia (Pape and Rose,
192 2023) and persistent depolarization of CA1 pyramidal cells after hypoxia combined with
193 glucose deprivation (Tanaka et al., 1997). The beginning of this postsynaptic failure coincides
194 with a surge of extracellular glutamate (**Fig. 2E**), which we attribute to the increase of
195 synaptic glutamate release at the onset of metabolic stress observed before (Hershkowitz et
196 al., 1993; Tanaka et al., 1997), and of extracellular potassium (**Fig. 1F, I**). Both are likely
197 driven by neuronal depolarization, Ca^{2+} accumulation and the various other contributing
198 mechanisms (Passlick et al., 2021). In contrast, shorter durations of chemical ischemia
199 durations lead to a transient failure of synaptic transmission, possibly due to a transient
200 depolarization of neurons, followed by an unexpected potentiation of synaptically-driven
201 glutamate transients and of postsynaptic responses.

202

203 ***Glutamate uptake is unaffected after acute chemical ischemia***

204 We next asked what the underlying reason for the increase glutamate transients is. One
205 potential explanation is a restriction of extracellular space (ECS): If a given amount of
206 glutamate is released into the ECS leading to a corresponding glutamate concentration, then
207 a reduction of the ECS would increase the glutamate concentration. Indeed, anoxia and

208 ischemia consistently lead to a reduction of the ECS fraction (Syková and Nicholson, 2008).
209 This scenario was investigated using the method of combining TMA-iontophoresis and TMA-
210 selective microelectrode recordings for estimating the ECS fraction and extracellular diffusion
211 (Nicholson, 1993; Hrabětová and Nicholson, 2007; Syková and Nicholson, 2008) in parallel
212 to chemical ischemia induction. We found that chemical ischemia with postsynaptic failure
213 was accompanied by a decreased ECS fraction and a decreased effective diffusion
214 coefficient, which is consistent with previous reports (Syková and Nicholson, 2008) (**Fig. S4**).
215 However, this was not observed for chemical ischemia without postsynaptic failure (**Fig. S4**),
216 in which the increased glutamate transients were observed.

217 An alternative explanation for the increased glutamate transients is reduced glutamate
218 uptake. To investigate this possibility, we analyzed the decay time constant of the iGluSnFR
219 fluorescence transients after synaptic stimulation, because it is increased when glutamate
220 uptake is decreased (Armbruster et al., 2016; Romanos et al., 2019). However, we did not
221 detect a significant change of the iGluSnFR decay time constant after chemical ischemia
222 (**Fig. 3A, B**). In addition, we tested if a deficit of glutamate uptake could be unmasked by
223 increasing the amount of synaptically released glutamate. This was tested by high-frequency
224 stimulation of CA3-CA1 synapses in the presence of glutamate receptor blockers (to prevent
225 induction of synaptic plasticity, **Fig. 3C**). Again, no differences of the decay time constant
226 were observed between control recordings and recordings with chemical ischemia (**Fig. 3E**).
227 Finally, we verified the sensitivity of our experimental approach by inhibiting glutamate uptake
228 pharmacologically at the end of the experiments. This manipulation indeed increased the
229 decay time constant by a factor of ~ 10-20 (**Fig. 3D, F, G**). We therefore conclude that
230 glutamate uptake is surprisingly resilient in the chemical ischemia model and that a reduction
231 of glutamate uptake does not explain the increased extracellular glutamate transients after
232 chemical ischemia without postsynaptic failure.

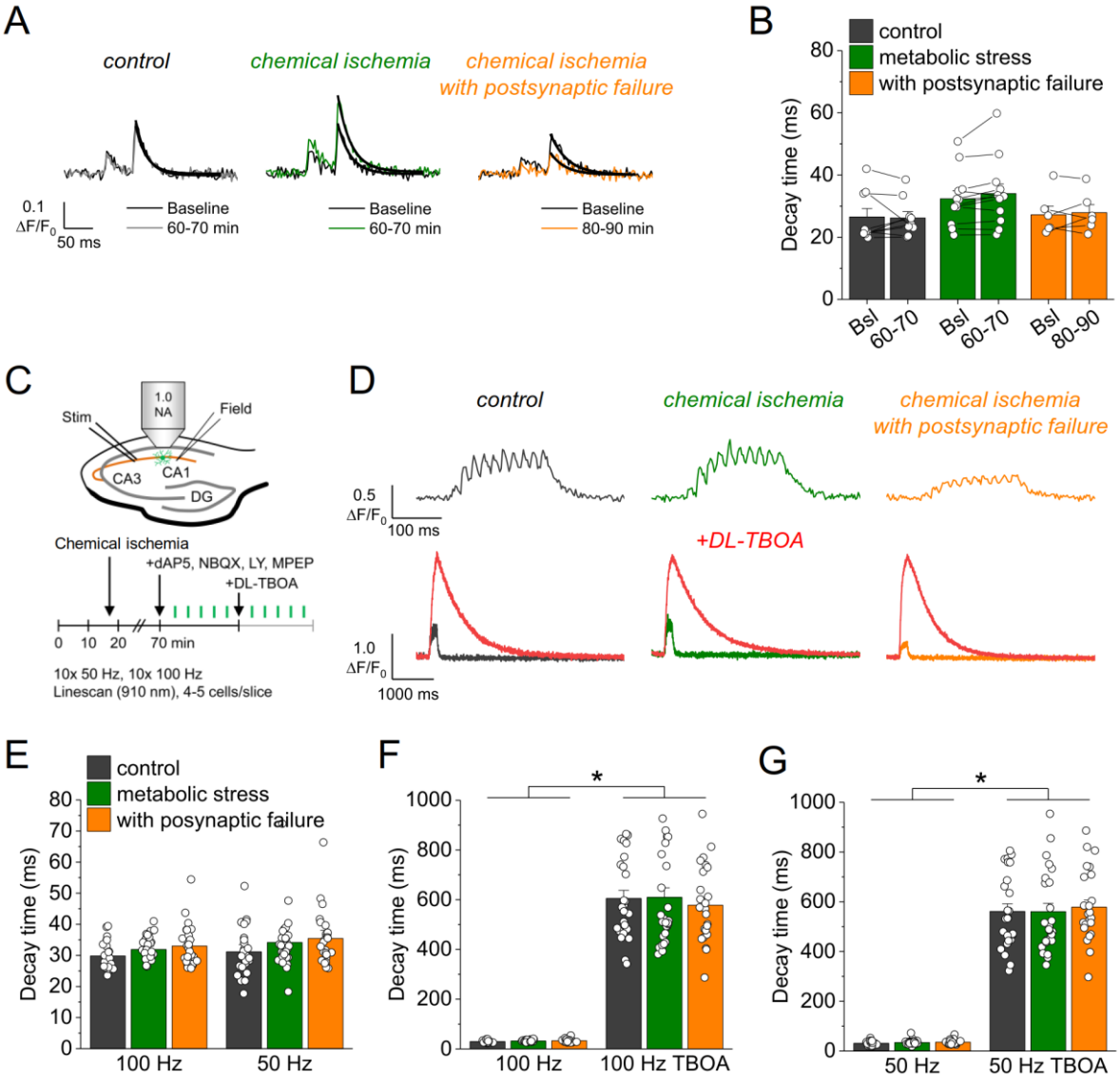

Figure 3: Glutamate clearance is not affected by transient chemical ischemia. (A) Example traces of iGluSnFR $\Delta F/F_0$ in response to paired-pulse stimulation (interstimulus interval 50 ms) during baseline (black) and last 10 min (60-70/80-90 min) of control (left, gray), chemical ischemia (middle, green) and chemical ischemia with postsynaptic failure (right, orange) recordings. Black line indicates exponential fit for the analysis of iGluSnFR decay time. (B) Quantification of iGluSnFR fluorescence decay time of the 2nd pulse of the paired-pulse stimulation during the last 10 min of recording (60-70/80-90 min) compared to baseline (Bsl) for control, chemical ischemia, and chemical ischemia with postsynaptic failure. Control: $p = 0.860$, $n = 9$; chemical ischemia, $p = 0.062$, $n = 12$; chemical ischemia with postsynaptic failure, $p = 0.648$, $n = 6$; paired Student's t-tests. (C) Schematic of experimental design. Combined recording of extracellular field potentials (Field) in the CA1 region in response to Schaffer collateral stimulation (Stim; paired pulse (50 ms), 0.05 Hz) and two-photon excitation fluorescence line scan imaging (910 nm) of iGluSnFR. After 70 min, D-AP5 (50 µM), NBQX (20 µM), LY341495 (50 µM) and MPEP (10 µM) were added to the recording solution and iGluSnFR fluorescence changes ($\Delta F/F_0$) were recorded in 4-5 cells in response to 10x 50 Hz and 10x 100 Hz stimulation before and after application of DL-TBOA (100 µM). (D) Example traces of iGluSnFR $\Delta F/F_0$

249 line scan recordings (average of 6 scans) in response to 10x 50 Hz stimulation (top row) after control
250 (left), chemical ischemia (middle) and chemical ischemia with postsynaptic failure recordings (right).
251 The same cells were tested again after block of glutamate transporters by DL-TBOA (bottom row, red
252 traces together with 'before' traces from upper row on different time scale for comparison). (E)
253 Quantification of iGluSnFR fluorescence decay time in response to 10x 100 Hz and 10x 50 Hz
254 stimulation after control, chemical ischemia recording without and with postsynaptic failure. 100 Hz: p
255 $= 0.060$, 50 Hz: $p = 0.149$; $n = 25$, 29, and 25 cells for control/chemical ischemia/chemical ischemia
256 with postsynaptic failure from 5, 6, and 5 independent experiments, respectively; Kruskal-Wallis
257 ANOVA. (F) Quantification of iGluSnFR fluorescence decay time in response to 10x 100 Hz
258 stimulation in the presence and absence of DL-TBOA (same cells as in E). $p < 0.0001$ for control,
259 chemical ischemia, and chemical ischemia with postsynaptic failure, paired sample Wilcoxon Signed
260 Ranks tests. (G) As in F but for 10x 50 Hz stimulation. $p < 0.0001$ for control, chemical ischemia, and
261 chemical ischemia with postsynaptic failure, paired sample Wilcoxon Signed Ranks tests. Data are
262 expressed as mean ± s.e.m.

263

264 ***Increased synaptic glutamate release after chemical ischemia***

265 Our results point towards an increased synaptic glutamate release when chemical ischemia
266 is shorter and followed by postsynaptic potentiation but not when it is associated with
267 postsynaptic failure. Investigating the paired-pulse behavior of synaptic responses is a
268 common approach for probing changes of presynaptic glutamate release (Debanne et al.,
269 1996). Analyzing the paired-pulse ratio (PPR) of postsynaptic response and iGluSnFR
270 transients revealed no consistent changes after chemical ischemia (**Fig. S5**). However, even
271 manifold presynaptically induced increases of synaptic strength were recently shown to result
272 in relatively small changes of the PPR, especially of the iGluSnFR signal at single CA3-CA1
273 synapses (Dürst et al., 2022). This suggests that a more moderate presynaptic increase of
274 glutamate release may escape its detection using the PPR. Therefore, we used an
275 electrophysiological approach that directly detects changes of the glutamate concentration in
276 the synaptic cleft. γ-D-glutamylglycine (γ-DGG) is a rapidly equilibrating competitive
277 antagonist of AMPA receptors, and its inhibitory effect on AMPA receptor mediated
278 postsynaptic responses depends on the ambient glutamate concentration because glutamate
279 and γ-DGG compete for AMPA receptor binding (Liu et al., 1999; Christie and Jahr, 2006):
280 The lower the glutamate concentration in the synaptic cleft, the stronger the inhibitory effect
281 of γ-DGG, and vice versa. For performing this test after chemical ischemia without
282 postsynaptic failure we combined our previous experimental approach with whole-cell patch
283 clamp recordings from CA1 pyramidal cells starting ~ 45 minutes after induction of chemical
284 ischemia (**Fig. 4A**). Analyzing the effect of γ-DGG application on simultaneously recorded
285 fEPSPs and excitatory postsynaptic currents (EPSCs), we found that the percentages of

286 fEPSP slopes and EPSC amplitudes remaining after γ-DGG were significantly higher in
287 experiments with chemical ischemia compared to control experiments (**Fig. 4B, C**). This
288 indicates that chemical ischemia led to an increased glutamate concentration in the synaptic
289 cleft, which is consistent with an increased synaptic glutamate release. Thus, shorter
290 durations of chemical ischemia led to a potentiation of presynaptic glutamate release and of
291 the postsynaptic response.

292

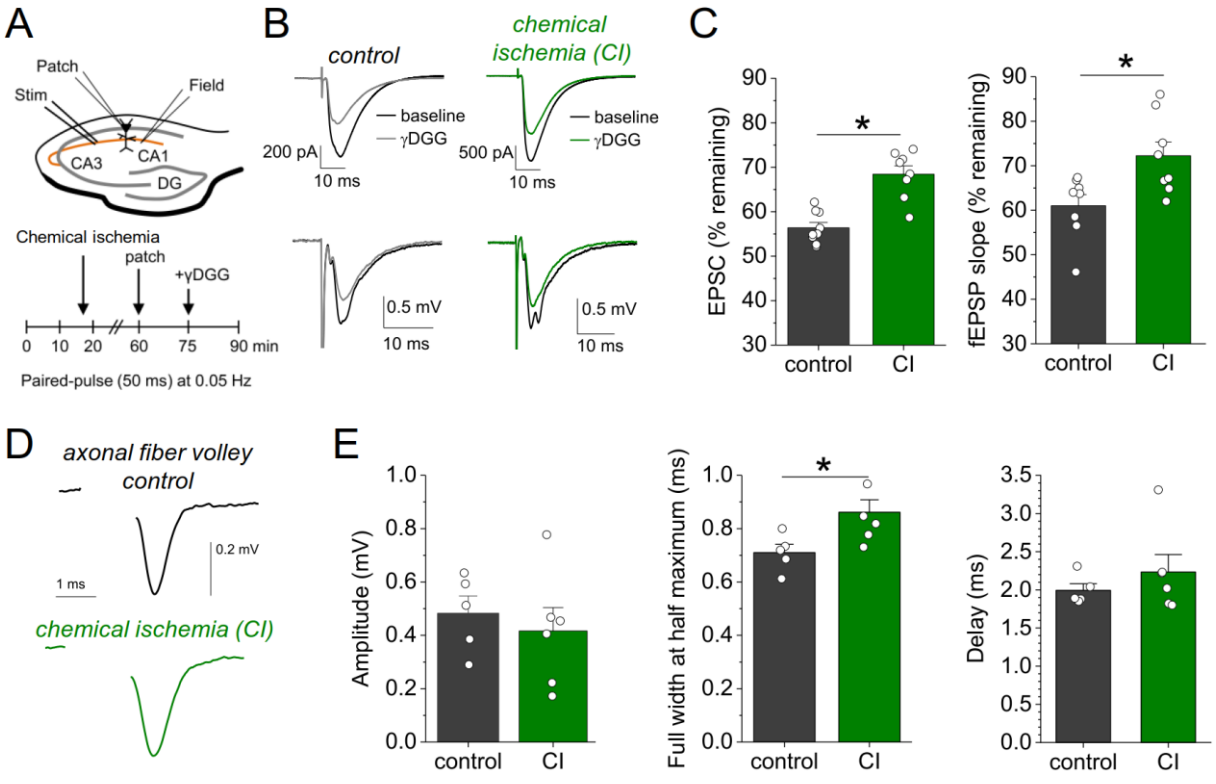

293

294 **Figure 4: Chemical ischemia increases synaptic glutamate release.** (A) Schematic of
295 experimental design. Extracellular field potentials (Field) were recorded in the CA1 region in response
296 to Schaffer collateral stimulation (Stim; paired pulse (50 ms), 0.05 Hz). After 60 min, a whole-cell patch
297 clamp recording from a CA1 pyramidal neuron was started. After recording baseline excitatory
298 postsynaptic current (EPSC) responses for 15 min, γDGG (1 mM) was added to the extracellular
299 solution. (B) Example traces of EPSCs (top) and fEPSPs (bottom) before (black) and after γDGG
300 application for control (left, gray) and chemical ischemia (right, green) recordings. (C) Quantification of
301 the remaining EPSC amplitude (left) and fEPSP slope (right) (in % of the baseline value) after γDGG
302 application for control (n = 9) and chemical ischemia (n = 8) recordings. EPSC, $p < 0.0001$; fEPSP, $p =$
303 0.014; paired two-sample Student's t-test. Data are expressed as mean ± s.e.m. (D) Example of
304 axonal fiber volleys from experiments shown in **Fig. 3C-E**. Stimulus artefact removed for clarity. (E)
305 Comparison of the fiber volley amplitude (left, $p = 0.57$), fiber volley half width at half maximum
306 (middle, $p = 0.026$) and fiber volley delay (time between onset of the stimulus and fiber volley peak,
307 right, $p = 0.39$). n = 5 (control) and 6 (chemical ischemia), unpaired Student's t-tests.

We further explored the underlying reason for this increase of glutamate release by computational modelling. First, we tested the hypothesis that presynaptic conditions expected for metabolic failure could increase vesicle loading with glutamate. This was tested using a previously established model for simulating presynaptic vesicle loading (Kolen et al., 2023). As shown in **Fig. S6**, accumulation of glutamate in the synaptic vesicle under control conditions reaches a steady state of close to 3,500 molecules. Cytosolic conditions consistent with metabolic failure (decreasing pH, increasing [Na^+] and [Cl^-], decreasing [K^+]) all lead to a smaller number of glutamate molecules in the vesicle. Similarly, a decrease in the extracellular pH and a reduced vesicular ATPase activity (due to reduced ATP levels) also cause a decrease in the luminal glutamate concentration. As a control, we increased the cytosolic pH from 7.2 to 7.4 and observed a significant rise in the number of glutamate molecules. However, we are not aware of any reports regarding a presynaptic alkalinization during ischemia or chemical ischemia. Overall, these simulations show that the conditions that are typically observed during ischemia or metabolic failure tend to lower the vesicular glutamate concentration and therefore cannot explain the observed increased glutamate release. An alternative explanation is an increased probability of presynaptic vesicular release, which could result from increased presynaptic Ca^{2+} influx, for instance, due to a presynaptic broadening of action potentials. For testing this, we analyzed the axonal fiber volley recorded in previous experiments (**Fig. 3C, D**), in which glutamate receptors were blocked and the fiber volley was therefore isolated (**Fig. 4D**). We found that the amplitude of the fiber volley was not different between control recordings and recordings after chemical ischemia without postsynaptic failure (**Fig. 4E**, left panel), which confirms previous conclusions (**Fig. 2**). However, the fiber volley was significantly broadened by ~ 20 % (**Fig. 4E**, middle panel) without a significant change of its delay after stimulation (**Fig. 4E**, right panel). This could indicate that short transient chemical ischemia broadens the presynaptic action potential, which increases presynaptic Ca^{2+} influx and presynaptic glutamate release and, as a consequence, the postsynaptic response.

Discussion

We modeled pathophysiological scenarios with transiently reduced ATP levels such as peri-infarct depolarizations (PIDs) and spreading depression (Lauritzen et al., 2011) by a chemical ischemia protocol. In our analysis, we focused on the recovery from this acute and transient chemical ischemia and its outcome. Depending on the duration of chemical ischemia, two qualitatively different changes of glutamatergic synaptic transmission became apparent. After prolonged chemical ischemia up to five minutes, the postsynaptic responses did not recover

344 in contrast to presynaptic action potential firing and presynaptic glutamate release, which,
345 however, did not completely return to baseline levels. After shorter chemical ischemia, the
346 postsynaptic responses and presynaptic glutamate release recovered and were potentiated
347 at the end of the recording whereas the axonal fiber volley amplitude was not different from
348 control recordings. Overall, these observations reveal a graded vulnerability of the involved
349 compartments to transient metabolic failure: Least resilient were postsynaptic neurons,
350 followed by presynaptic glutamate release and axonal action potential firing. In contrast,
351 glutamate clearance, which is mostly due to astrocytic glutamate uptake (Danbolt, 2001),
352 was mostly unaffected even after long durations of chemical ischemia. This is in line with the
353 observation from the hippocampus that transient chemical ischemia triggers much smaller
354 ATP decreases and Na^+ increases, a measure of dysregulation of ion homeostasis, in
355 astrocytes compared to neurons (Meyer et al., 2022; Pape and Rose, 2023). This is because
356 of the strong expression of postsynaptic neuronal N-methyl-D-aspartate receptors (NMDARs)
357 and TRPV4 (Pape and Rose, 2023). It is also noteworthy that presynaptic glutamate release
358 recovered to some extent even if the postsynaptic neurons remained unresponsive, thereby
359 masking the recovery of glutamate release. We have not systematically tested durations of
360 chemical ischemia beyond five minutes, because it is safe to assume this would further slow
361 down, and ultimately prevent, the recovery of glutamate release and eventually also impair
362 axonal action potential firing (**Fig. 2E**).

363 The persistent potentiation of glutamate release after short chemical ischemia was
364 unexpected. It was detected in electrophysiological recording using γ-DGG and iGluSnFR
365 fluorescence imaging and it was not caused by a reduced glutamate uptake or changes of
366 the extracellular space. Instead, a likely explanation is a broadening of presynaptic axonal
367 action potentials, which is strongly suggested by the widened fiber volley in the absence of
368 changes of fiber volley amplitude or delay. Nonetheless, a widened fiber volley could also be
369 explained by, for instance, a desynchronization of presynaptic action potential firing.
370 Presynaptic action potential broadening could explain increased glutamate release, because
371 pharmacological prolongation of presynaptic action potentials by 4-AP was previously shown
372 to increase postsynaptic responses by increasing presynaptic Ca^{2+} influx at these synapses
373 (Wheeler et al., 1996; Qian and Saggau, 1999). A potential reason for the action potential
374 widening is an inactivation of potassium currents (Mitterdorfer and Bean, 2002), because of a
375 lasting depolarization after transient chemical ischemia. Whether this is indeed the case
376 remains to be tested experimentally. Alternatively, short durations of chemical ischemia could
377 increase presynaptic glutamate release by persistently altering the presynaptic resting
378 concentration of Ca^{2+} (Eshra et al., 2021) or presynaptic cAMP signaling (Vaden et al., 2019),
379 which are only two prominent examples among many others.

380 The time course of the potentiation of glutamate release and of the postsynaptic response
381 were almost identical (**Fig. 2D**), which could suggest that the increased presynaptic release
382 directly leads to the potentiation of the postsynaptic response. It has previously been shown
383 that the potentiation of synaptic transmission (LTP) in ischemia models (ischemic/anoxic
384 LTP) and physiological LTP can occlude each other (Hsu and Huang, 1997; Stein et al.,
385 2015), which indicates that they can share the mechanisms underlying the potentiation of
386 synaptic transmission. For CA3-CA1 synapses, there is a long-standing debate to what
387 extent and under which conditions postsynaptic mechanisms such as receptor insertion and
388 presynaptic changes of release underlie LTP (Padamsey and Emptage, 2014). Our
389 experiments suggest that the potentiation of postsynaptic responses is at least in part due to
390 increased glutamate release, but they also do not rule out a mix of pre- and postsynaptic
391 changes.

392 Glutamate uptake can be used as an indirect measure of the astrocytic metabolic status,
393 because it is mostly mediated by astrocytes and driven by their transmembrane Na^+ gradient
394 and membrane potential (Danbolt, 2001; Rossi et al., 2007; Passlick et al., 2021), which are
395 maintained by the Na^+/K^+-ATPase. In experiments with prolonged chemical ischemia with
396 postsynaptic failure, we observed preserved glutamate uptake in two thirds of the
397 experiments whereas in one third iGluSnFR expressed by astrocytes disappeared after
398 chemical ischemia. While we do not know the exact reason for the latter, astrocyte
399 metabolism seems to be overall more resilient to transient ischemia than the postsynaptic
400 cells. In experiments without postsynaptic failure, no lasting reduction of glutamate uptake
401 was detected. Neither observation rules out that glutamate uptake was transiently impaired
402 during or immediately following chemical ischemia, because in this time period astrocytic Na^+
403 levels were shown to increase reversibly (Gerkau et al., 2018; Pape and Rose, 2023).
404 Similarly, they do not rule out that astrocytes are a transient source of glutamate during
405 chemical ischemia by, for instance, reverse transport and channel-mediated glutamate
406 release (Rossi et al., 2000, 2007; Yang et al., 2019; Passlick et al., 2021). Taken together,
407 lasting effects of chemical ischemia on glutamate uptake were insignificant compared to
408 changes of presynaptic glutamate release and synaptic transmission.

409 In summary, our experiments reveal a bidirectional dysregulation of glutamate signaling after
410 transient metabolic failure. Especially the lasting potentiation of synaptic glutamate release
411 after short periods of energy depletion could be an important new aspect in the disease
412 context. If individual PIDs lead to a similar potentiation of glutamate release, the latter could
413 promote excitotoxic damage in the peri-infarct tissue. However, our experiments using
414 chemical ischemia in acute hippocampal slices do not fully reproduce the complex situation
415 in the brain during stroke or PIDs, of course. While our approach allowed us to investigate

the effect of variable degrees of cellular ATP depletion (Pape and Rose, 2023) on glutamatergic synapse function and to dissect the relevant cellular and synaptic mechanisms in detail, it investigates cellular changes independent of, for instance, blood circulation and the constraints imposed by a fixed skull volume. Another variable that could be of interest is sex, because many aspects of glutamate signaling such as receptor and transporter expression can depend on sex and/or estrous cycle (Giacometti and Barker, 2020). In the present study, we have performed experiment exclusively on male mice, leaving the question of a sex-dependence of our observation unanswered. It will be interesting to understand, if such factors modify the bidirectional dysregulation of glutamate signaling observed here.

Acknowledgements

We thank Gerald Seifert and Thomas Erdmann for support with animal breeding and maintenance and Temitope Adeoye for useful discussion on synaptic vesicle release. The study was supported by the German Research Foundation (DFG, FOR2795, to C.H.) and the National Institutes of Health (Grant number R01NS130916, to G.U.).

Author contributions: S.P. performed and analyzed all electrophysiological and imaging experiments. Modelling of glutamate transport was done by G.U. C.H. conceived the study, analyzed data, and wrote the initial version of the manuscript, to which all authors subsequently contributed.

Competing Interest Statement: There are no competing interests.

Keywords: glutamatergic synaptic transmission, glutamate clearance, chemical ischemia, ischemia, hippocampus.

Materials and Methods

Animals

Experiments were performed using 2-4-months-old male C57BL/6N mice (Charles River) that were kept under 12 h light/dark conditions and had *ad libitum* access to food and water. All animal procedures were conducted in accordance with the regulations of the European Commission Directive 2010/63/EU and all relevant national and institutional guidelines and requirements. Procedures were further approved by the Landesamt für Natur, Umwelt und Verbraucherschutz Nordrhein-Westfalen (LANUV, Recklinghausen, Germany) where required.

Stereotactic injections

In order to express the glutamate sensor iGluSnFR (Marvin et al., 2013) on the surface of astrocytes, 4-weeks-old C57BL/6N mice were injected bilaterally with an AAV expressing iGluSnFR under control of the GFAP promoter (AAV1.GFAP.iGluSnFr.WPRE.SV40, PennCore) into the CA1 region of the dorsal hippocampus. Mice were deeply anesthetized by intraperitoneal injection (i.p.) of Fentanyl/Midazolam/Medetomidin (0.05/5.0/0.5 mg/kg bodyweight, injection volume 0.1 ml/10 g bodyweight). After deep anesthesia was confirmed, the head was shaved, the skin disinfected, and the head fixed in a stereotactic frame (Model 901, David Kopf Instruments). An incision was made, bregma localized, and a small hole was drilled with a dental drill (coordinates for the dorsal hippocampus, relative to bregma: anterior −1.8 mm, lateral +/− 1.6 mm, ventral −1.6 mm). Next, a beveled needle nanosyringe (nanofil 34 G BVLD, WPI) was slowly inserted into the brain and 0.5 to 1 µl of viral particles were injected into the hippocampus using a microinjection pump (50 nl/min, WPI). The injection needle was left in place for about 3 minutes and then slowly retracted. After repeating the procedure for the other hemisphere, the incision was sutured using absorbable thread (Ethicon) and an antibiotic was applied (Refobacin 1 mg/g, Gentamicin). Finally, anesthesia was terminated by i.p. injection of Naloxon/Flumazenil/Atipamezol (1.2/0.5/2.5 mg/kg bodyweight, injection volume 0.1 ml/10 g bodyweight). Analgesia was applied 30 min before terminating the anesthesia and 24 h after surgery by subcutaneous injection of carprofen (5 mg/kg bodyweight, injection volume 0.1 ml/20 g bodyweight). Animals were used for experiments 2–5 weeks after virus injection.

Hippocampal slice preparation

474 Electrophysiology and two-photon excitation fluorescence microscopy in acute hippocampal
475 slices were combined as previously described (Minge et al., 2017). Briefly, coronal slices
476 were obtained from mice and virus-injected mice (see above) with a thickness of 300 µm.
477 Slices were prepared in an ice-cold slicing solution containing (in mM): NaCl 60, sucrose
478 105, KCl 2.5, $MgCl_2$ 7, NaH_2PO_4 1.25, ascorbic acid 1.3, sodium pyruvate 3, $NaHCO_3$ 26,
479 $CaCl_2$ 0.5, and glucose 10 (osmolarity 300-310 mOsm/l), and kept in the slicing solution at
480 34°C for 15 minutes before being stored at room temperature (21-23 °C) in an artificial
481 cerebral spinal fluid (ACSF) containing (in mM): NaCl 131, KCl 2.5, $MgSO_4$ 1.3, $CaCl_2$ 2,
482 NaH_2PO_4 1.25, $NaHCO_3$ 21, and glucose 10 (osmolarity adjusted to 295-305 mOsm/l). Slices
483 were allowed to rest for at least 60 minutes. For recordings, slices were transferred to a
484 submersion-type recording chamber and perfused with extracellular solution (ACSF). All
485 recordings were performed at 33-35 °C. All solutions were continuously bubbled with 95%
486 O_2/ 5% CO_2. The flow rate of the extracellular solution was kept constant at 6-7 ml/min
487 throughout all experiments.

488

489 ***Electrophysiology***

490 Extracellular recordings of field excitatory postsynaptic potentials (fEPSPs) were performed
491 using patch pipettes filled with extracellular solution placed in the stratum radiatum of the
492 CA1 region. For stimulation of CA3-CA1 Schaffer collateral axonal connections, a bipolar
493 concentric stimulation electrode was placed in the stratum radiatum at the border between
494 CA2/3 and CA1. Stimulation intensities (DS3, Digitimer Ltd., UK) were set to obtain ~ 50% of
495 the maximum fEPSP amplitude. The duration of individual stimuli was 100 µs. In some
496 experiments, field recordings were combined with whole-cell patch clamp recordings from
497 CA1 pyramidal cells using standard patch pipettes (3-4 MΩ) filled with an intracellular
498 solution containing (in mM): KCH_3O_3S 135, HEPES 10, di-Tris-Phosphocreatine 10, $MgCl_2$ 4,
499 Na_2-ATP 4, Na-GTP 0.4, 0.2 BAPTA, 5 QX314-Cl (pH adjusted to 7.2, osmolarity 290-295
500 mOsm/l). CA1 pyramidal cells were identified using infrared differential interference contrast
501 or Dodt contrast optics by their typical morphology and location. Data were recorded using
502 MultiClamp 700B (Molecular Devices) amplifiers, digitized (10 kHz) and stored for offline
503 analysis. Whole-cell patch clamp recordings were rejected if at any time the access
504 resistance exceeded 25 MΩ or changed by more than 20%.

505 Acute chemical ischemia was induced by switching from normal ACSF to a modified ACSF
506 with 0 mM glucose, 2 mM deoxyglucose (2-DG) to inhibit ATP production through glycolysis,
507 and 5 mM sodium azide (NaN_3) to inhibit ATP production through oxidative phosphorylation.
508 The modified ACSF was applied for variable durations ranging from 2 to 5 minutes. In some

experiments, the inhibitors D-AP5 (dAP5 in figures, 50 µM, Abcam), NBQX disodium salt (10 µM, Abcam), DL-TBOA (100 µM, Tocris), LY341495 (50 µM, Tocris), MPEP (10 µM, Tocris), and/or γ-DGG (1 mM, Tocris) were added to the extracellular solution as indicated.

Glutamate imaging using iGluSnFR

Glutamate imaging using iGluSnFR (Marvin et al., 2013) in combination with electrophysiology was performed similarly as previously described (Herde et al., 2020). Slices with astrocytes expressing iGluSnFR after viral injection (see above) were transferred to a submersion-type recording chamber mounted on a Scientifica two-photon excitation fluorescence microscope with a 60x/1.0 NA objective (Olympus). iGluSnFR was excited using a femtosecond pulse laser (Vision S, Coherent, excitation wavelength of 910 nm). During imaging, line scans of iGluSnFR fluorescence were repeatedly obtained. The scanned line was positioned in the periphery of an iGluSnFR-expressing astrocytes (for example Fig. 2B). The line was scanned at a frequency of 378.8 Hz to obtain a fluorescence profile over time. Line scans were repeated 4-6 times for each individual time point and experiment and averaged before the background fluorescence was subtracted to obtain an average iGluSnFR fluorescence time course. The resting iGluSnFR fluorescence before synaptic stimulation (F_0), the maximum change of iGluSnFR fluorescence (ΔF_{MAX}) and the normalized iGluSnFR time course ($\Delta F/F_0$) were determined. iGluSnFR imaging was combined with paired synaptic stimuli (Fig. 2), high-frequency synaptic stimulation (Fig. 3), and iontophoretic glutamate application (Suppl. Fig. 2). For the latter, an iontophoretic application system (MVCS-02C-150, NPI) was used with iontophoretic pipettes (60-80 MΩ resistance) filled with 150 mM glutamic acid (pH adjusted to 7.0 with NaOH) and 40 µM Alexa Fluor 633 to localize the pipette.

Measurements of extracellular space fraction and diffusivity and extracellular K^+

Extracellular [K^+] was recorded using K^+-sensitive microelectrodes as previously described (Breithausen et al., 2020). Briefly, these microelectrodes were built using theta-glass capillaries and pulled with a horizontal pipette puller. The reference and the K^+-sensitive barrel were filled with a NaCl (154 mM) and KCl (150 mM) solution, respectively. The tip of the K^+-sensitive barrel was filled with a valinomycin-based K^+ ionophore (K^+ ionophore 1, cocktail B, Sigma-Aldrich). The K^+-sensitive microelectrodes were calibrated before each experiment with solutions containing 154 mM NaCl and 3 or 30 mM KCl. Electrodes were used if they responded to this 10x increase of K+ with a voltage response > 50 mV.

543 Measurements of the relative changes of the extracellular space (ECS) fraction and of
544 extracellular diffusion during experiments with acute chemical ischemia were obtained using
545 the method of combining tetramethylammonium (TMA) iontophoresis and TMA-sensitive
546 electrodes recordings (Nicholson, 1993; Hrabětová and Nicholson, 2007; Syková and
547 Nicholson, 2008). TMA-sensitive, double-barrel microelectrodes were built like K^+-sensitive
548 microelectrodes except that the TMA-sensitive ionophore solution (IE190, WPI) and 150 mM
549 TMA chloride, as the intrapipette solution, were used for the TMA-sensitive barrel. The
550 reference barrel was filled with 154 mM NaCl and 60 μM Alexa Fluor 594 to visualize the
551 electrode. Recordings were performed using an ION-01M amplifier (NPI, Germany). TMA-
552 sensitive microelectrodes were tested for their sensitivity to TMA before each experiment by
553 two calibration solutions containing either (in mM) TMA 1, KCl 3, NaCl 150 or TMA 10, KCl 3,
554 NaCl 141. Only electrodes that responded to this 10-fold increase of TMA with a potential
555 increase of > 50 mV were used for the experiments. A subset of electrodes was also tested
556 for their sensitivity over a larger range of TMA concentrations, which revealed Nernst-like
557 behavior over higher concentrations and only a departure from that in the low sub-millimolar
558 range. To correct for that, the calibration curve was fitted with the Nicolsky-Eisenman
559 equation and the conversion of the TMA-electrode potential into a TMA concentration was
560 adapted accordingly (Nicholson, 1993). For recordings in chemical ischemia experiments
561 (Suppl. Fig. 3), the TMA-sensitive microelectrode was placed into the CA1 stratum radiatum
562 and an iontophoresis pipette filled with 100 mM TMA and 60 μM Alexa Fluor 594 was placed
563 at distance of 100-200 μm from the TMA-sensitive microelectrode. At each time point during
564 the recording, TMA was iontophoretically injected into the tissue (100 nA, 30 s) and the
565 corresponding [TMA] time course was calculated. For examples, see Suppl. Fig. 3. Each
566 time course was fitted using equations 10.2 to 10.4 from (Hrabětová and Nicholson, 2007)
567 using a MATLAB script to obtain the extracellular space (ECS) fraction and the effective TMA
568 diffusion coefficient (D*). D* deviates from the free diffusion coefficient of TMA (D) because
569 the tortuosity of the ECS reduces TMA diffusion over the distances investigated here
570 (Hrabětová and Nicholson, 2007). Therefore, changes of D* can indicate a change of ECS
571 tortuosity. In these experiments, the extracellular solution always contained 1 mM TMACl to
572 provide a known basal extracellular TMA concentration for the conversion of the recorded
573 microelectrode potential into [TMA]. The reference barrel of the TMA-sensitive
574 microelectrode was also used for recording fEPSPs in response to axonal stimulation. We
575 have verified these recordings to report accurate values by recording [TMA] transients in
576 agarose gel (ECS fraction ~ 1, tortuosity ~ 1) (Nicholson, 1993) and in acute brain slices, in
577 which we obtained an ECS fraction of 0.19 ± 0.023 (n = 5) and a tortuosity of 1.54 ± 0.046 (n
578 = 5) and which matches previous measurements in this region (Nicholson, 1993; Syková and
579 Nicholson, 2008)

Glutamate accumulation in synaptic vesicles

The accumulation of glutamate in synaptic vesicles is modeled as previously described (Kolen et al., 2023) and the code for the model is archived along with it. Briefly, the temporal evolution of luminal glutamate molecule number, [H^+], pH, and [Cl^-] are modeled by the following rate equations:

$$\frac{d[Glut]_L}{dt} = J_{VGLUT}, \tag{1}$$

$$\frac{d[H^+]_L}{dt} = J_{H^+} + J_{V_{ATPase}} - J_{VGLUT}, \tag{2}$$

$$\frac{dpH_L}{dt} = -\frac{1}{N_A}\left(\frac{dH_L^+}{dt}\frac{1}{V}\right)\left(\frac{1}{\beta_{pH}}\right), \tag{3}$$

$$\frac{d[Cl^-]_L}{dt} = J_{VGLUT_{Cl}}. \tag{4}$$

Where N_A, β_{pH} (= $\frac{40\ mM}{pH}$), and V represent Avogadro's number, the pH-buffering capacity of the vesicle, and the vesicle volume assuming a radius of 20 nm. The equations for glutamate/H^+ flux through glutamate transporters (J_{VGLUT}), Cl^- flux through glutamate transporters ($J_{VGLUT_{Cl}}$), proton leak (J_{H^+}), and V-type ATPase ($J_{V_{ATPase}}$) are described in (Kolen et al., 2023).

The equation for the membrane potential of the vesicle ($\Delta\psi$) is,

$$\Delta\psi = \frac{F\times V}{C}([H^+]_L + [K^+]_L + [Na^+]_L - [Cl^-]_L - [Glut]_L - B) \tag{5}$$

with $C = C_0 \times S$ being the total capacitance of the vesicle with C_0= 1 μF/cm^2, S the surface area of the vesicle, and F Faraday's constant. Luminal K^+ ($[K^+]_L$) and Na^+ ($[Na^+]_L$) concentrations were fixed to extracellular values, i.e. to 5 mM and 145 mM, respectively. B is the luminal concentration of impermeant charges given by the conservation of charge in the vesicle under initial conditions (indicated by the subscript 0).

$$B = [H^+]_{L,0} + [K^+]_{L,0} + [Na^+]_{L,0} - [Cl^-]_{L,0} - [Glut]_{L,0} - \frac{C}{F\times V}(\psi_{in} - \psi_{out}) \tag{6}$$

Finally, the effect of surface charge on various ion concentrations at the membrane was also taken into account, with the inner (ψ_{in}) and outer (ψ_{out}) leaflets potentials set to 0 mV and -50 mV, respectively.

Starting conditions for the mathematical modeling reflect the ion concentrations immediately after endocytosis of synaptic vesicles: the vesicular lumen contained solutions resembling the external solutions, with high [Cl^-], neutral pH and negligible glutamate concentration ($[K^+]_{L,0}$= 5 mM, $[Na^+]_{L,0}$ = 145 mM, $[Cl^-]_{L,0}$ = 110 mM, $[\mathrm{Glut}]_{L,0}$ = 1 μM, and $pH_{L,0}$ = 7.2);

610 cytoplasmic pH, Cl^-, K^+, Na^+, and glutamate concentration was set to 7.2, 10 mM, 140 mM,
611 10 mM, and 10 mM, respectively. We also incorporated changes in luminal Na^+ and K^+
612 concentrations, however, both did not affect our results.

613

614 ***Statistics***

615 Analyses were performed using ImageJ (NIH), Origin (OriginLab) and Matlab (MathWorks).
616 Numerical data are reported as mean ± s.e.m. with n being the number of samples. In all
617 electrophysiological and imaging experiments in acute hippocampal slices, n refers to the
618 number of recordings. was typically performed per acute hippocampal slice. Because the
619 success rate of experiments combining electrophysiology, two-photon excitation imaging and
620 pharmacology is low, a single successful experiment was typically performed per day and
621 animal. For all other experimental designs, detailed information can be found in the figure
622 legends. The Shapiro-Wilk test was used to establish if data were normally distributed.
623 Comparisons were then performed using the appropriate parametric and non-parametric
624 tests (e.g., Student's t-test or Mann-Whitney U-test). The statistical tests used are indicated
625 throughout. In figures, asterisks indicate significance levels where *** indicated $p < 0.001$, **
626 $p < 0.01$ and * $p < 0.05$, error bars represent s.e.m. and dots represent individual data points,
627 which are connected by lines for paired data points.

628

References

Armbruster, M., Hanson, E., and Dulla, C. G. (2016). Glutamate Clearance Is Locally Modulated by Presynaptic Neuronal Activity in the Cerebral Cortex. *J. Neurosci.* 36, 10404–10415. doi: 10.1523/JNEUROSCI.2066-16.2016

Breithausen, B., Kautzmann, S., Boehlen, A., Steinhäuser, C., and Henneberger, C. (2020). Limited contribution of astroglial gap junction coupling to buffering of extracellular K+ in CA1 stratum radiatum. *Glia* 68, 918–931. doi: 10.1002/glia.23751

Christie, J. M., and Jahr, C. E. (2006). Multivesicular Release at Schaffer Collateral–CA1 Hippocampal Synapses. *J Neurosci* 26, 210–216. doi: 10.1523/JNEUROSCI.4307-05.2006

Crepel, V., Epsztein, J., and Ben-Ari, Y. (2003). Ischemia induces short- and long-term remodeling of synaptic activity in the hippocampus. *J. Cell. Mol. Med.* 7, 401–407. doi: 10.1111/j.1582-4934.2003.tb00242.x

Crepel, V., Hammond, C., Chinestra, P., Diabira, D., and Ben-Ari, Y. (1993). A selective LTP of NMDA receptor-mediated currents induced by anoxia in CA1 hippocampal neurons. *J. Neurophysiol.* 70, 2045–2055. doi: 10.1152/jn.1993.70.5.2045

Danbolt, N. C. (2001). Glutamate uptake. *Prog. Neurobiol.* 65, 1–105.

Debanne, D., Guérineau, N. C., Gähwiler, B. H., and Thompson, S. M. (1996). Paired-pulse facilitation and depression at unitary synapses in rat hippocampus: quantal fluctuation affects subsequent release. *J. Physiol.* 491, 163–176. doi: 10.1113/jphysiol.1996.sp021204

Dirnagl, U., Iadecola, C., and Moskowitz, M. A. (1999). Pathobiology of ischaemic stroke: an integrated view. *Trends Neurosci.* 22, 391–397. doi: 10.1016/S0166-2236(99)01401-0

Dürst, C. D., Wiegert, J. S., Schulze, C., Helassa, N., Török, K., and Oertner, T. G. (2022). Vesicular release probability sets the strength of individual Schaffer collateral synapses. *Nat Commun* 13, 6126. doi: 10.1038/s41467-022-33565-6

Eshra, A., Schmidt, H., Eilers, J., and Hallermann, S. (2021). Calcium dependence of neurotransmitter release at a high fidelity synapse. *eLife* 10, e70408. doi: 10.7554/eLife.70408

Gerkau, N. J., Rakers, C., Durry, S., Petzold, G. C., and Rose, C. R. (2018). Reverse NCX Attenuates Cellular Sodium Loading in Metabolically Compromised Cortex. *Cereb Cortex* 28, 4264–4280. doi: 10.1093/cercor/bhx280

Giacometti, L., and Barker, J. (2020). Sex differences in the glutamate system: Implications for addiction. *Neuroscience & Biobehavioral Reviews* 113, 157–168. doi: 10.1016/j.neubiorev.2020.03.010

Herde, M. K., Bohmbach, K., Domingos, C., Vana, N., Komorowska-Müller, J. A., Passlick, S., et al. (2020). Local Efficacy of Glutamate Uptake Decreases with Synapse Size. *Cell Rep.* 32, 108182. doi: 10.1016/j.celrep.2020.108182

Hershkowitz, N., Katchman, A. N., and Veregge, S. (1993). Site of synaptic depression during hypoxia: a patch-clamp analysis. *Journal of Neurophysiology* 69, 432–441. doi: 10.1152/jn.1993.69.2.432

670 Hrabětová, S., and Nicholson, C. (2007). “Biophysical Properties of Brain Extracellular Space
671 Explored with Ion-Selective Microelectrodes, Integrative Optical Imaging and Related
672 Techniques,” in *Electrochemical Methods for Neuroscience*, eds. A. C. Michael and L.
673 M. Borland (Boca Raton (FL): CRC Press/Taylor & Francis).

674 Hsu, K.-S., and Huang, C.-C. (1997). Characterization of the anoxia-induced long-term
675 synaptic potentiation in area CA1 of the rat hippocampus. *British Journal of*
676 *Pharmacology* 122, 671–681. doi: 10.1038/sj.bjp.0701409

677 Kolen, B., Borghans, B., Kortzak, D., Lugo, V., Hannack, C., Guzman, R. E., et al. (2023).
678 Vesicular glutamate transporters are H+-anion exchangers that operate at variable
679 stoichiometry. *Nat Commun* 14, 2723. doi: 10.1038/s41467-023-38340-9

680 Lauritzen, M., Dreier, J. P., Fabricius, M., Hartings, J. A., Graf, R., and Strong, A. J. (2011).
681 Clinical Relevance of Cortical Spreading Depression in Neurological Disorders:
682 Migraine, Malignant Stroke, Subarachnoid and Intracranial Hemorrhage, and
683 Traumatic Brain Injury. *J Cereb Blood Flow Metab* 31, 17–35. doi:
684 10.1038/jcbfm.2010.191

685 Liu, G., Choi, S., and Tsien, R. W. (1999). Variability of neurotransmitter concentration and
686 nonsaturation of postsynaptic AMPA receptors at synapses in hippocampal cultures
687 and slices. *Neuron* 22, 395–409.

688 Marvin, J. S., Borghuis, B. G., Tian, L., Cichon, J., Harnett, M. T., Akerboom, J., et al. (2013).
689 An optimized fluorescent probe for visualizing glutamate neurotransmission. *Nat.*
690 *Methods* 10, 162–170. doi: 10.1038/nmeth.2333

691 Meyer, J., Gerkau, N. J., Kafitz, K. W., Patting, M., Jolmes, F., Henneberger, C., et al. (2022).
692 Rapid Fluorescence Lifetime Imaging Reveals That TRPV4 Channels Promote
693 Dysregulation of Neuronal Na+ in Ischemia. *J. Neurosci.* 42, 552–566. doi:
694 10.1523/JNEUROSCI.0819-21.2021

695 Mies, G., and Paschen, W. (1984). Regional changes of blood flow, glucose, and ATP
696 content determined on brain sections during a single passage of spreading
697 depression in rat brain cortex. *Experimental Neurology* 84, 249–258. doi:
698 10.1016/0014-4886(84)90222-X

699 Minge, D., Senkov, O., Kaushik, R., Herde, M. K., Tikhobrazova, O., Wulff, A. B., et al.
700 (2017). Heparan Sulfates Support Pyramidal Cell Excitability, Synaptic Plasticity, and
701 Context Discrimination. *Cereb. Cortex* 27, 903–918. doi: 10.1093/cercor/bhx003

702 Mitterdorfer, J., and Bean, B. P. (2002). Potassium Currents during the Action Potential of
703 Hippocampal CA3 Neurons. *J. Neurosci.* 22, 10106–10115.

704 Nicholson, C. (1993). Ion-selective microelectrodes and diffusion measurements as tools to
705 explore the brain cell microenvironment. *J. Neurosci. Methods* 48, 199–213. doi:
706 10.1016/0165-0270(93)90092-6

707 Padamsey, Z., and Emptage, N. (2014). Two sides to long-term potentiation: a view towards
708 reconciliation. *Philosophical Transactions of the Royal Society B: Biological Sciences*
709 369, 20130154. doi: 10.1098/rstb.2013.0154

710 Pape, N., and Rose, C. R. (2023). Activation of TRPV4 channels promotes the loss of cellular
711 ATP in organotypic slices of the mouse neocortex exposed to chemical ischemia. *The*
712 *Journal of Physiology* 601, 2975–2990. doi: 10.1113/JP284430

Passlick, S., Rose, C. R., Petzold, G. C., and Henneberger, C. (2021). Disruption of Glutamate Transport and Homeostasis by Acute Metabolic Stress. *Front Cell Neurosci* 15, 637784. doi: 10.3389/fncel.2021.637784

Qian, J., and Saggau, P. (1999). Modulation of Transmitter Release by Action Potential Duration at the Hippocampal CA3-CA1 Synapse. *J. Neurophysiol.* 81, 288–298. doi: 10.1152/jn.1999.81.1.288

Rakers, C., and Petzold, G. C. (2017). Astrocytic calcium release mediates peri-infarct depolarizations in a rodent stroke model. *J Clin Invest* 127, 511–516. doi: 10.1172/JCI89354

Romanos, J., Benke, D., Saab, A. S., Zeilhofer, H. U., and Santello, M. (2019). Differences in glutamate uptake between cortical regions impact neuronal NMDA receptor activation. *Commun Biol* 2, 1–15. doi: 10.1038/s42003-019-0367-9

Rossi, D. J., Brady, J. D., and Mohr, C. (2007). Astrocyte metabolism and signaling during brain ischemia. *Nat. Neurosci.* 10, 1377–1386. doi: 10.1038/nn2004

Rossi, D. J., Oshima, T., and Attwell, D. (2000). Glutamate release in severe brain ischaemia is mainly by reversed uptake. *Nature* 403, 316–321. doi: 10.1038/35002090

Stein, E. S., Itsekson-Hayosh, Z., Aronovich, A., Reisner, Y., Bushi, D., Pick, C. G., et al. (2015). Thrombin induces ischemic LTP (iLTP): implications for synaptic plasticity in the acute phase of ischemic stroke. *Sci. Rep.* 5, 7912. doi: 10.1038/srep07912

Syková, E., and Nicholson, C. (2008). Diffusion in Brain Extracellular Space. *Physiol. Rev.* 88, 1277–1340. doi: 10.1152/physrev.00027.2007

Tanaka, E., Yamamoto, S., Kudo, Y., Mihara, S., and Higashi, H. (1997). Mechanisms Underlying the Rapid Depolarization Produced by Deprivation of Oxygen and Glucose in Rat Hippocampal CA1 Neurons In Vitro. *Journal of Neurophysiology* 78, 891–902. doi: 10.1152/jn.1997.78.2.891

Vaden, J. H., Banumurthy, G., Gusarevich, E. S., Overstreet-Wadiche, L., and Wadiche, J. I. (2019). The readily-releasable pool dynamically regulates multivesicular release. *eLife* 8, e47434. doi: 10.7554/eLife.47434

Wheeler, D. B., Randall, A., and Tsien, R. W. (1996). Changes in action potential duration alter reliance of excitatory synaptic transmission on multiple types of Ca2+ channels in rat hippocampus. *J. Neurosci.* 16, 2226–2237. doi: 10.1523/JNEUROSCI.16-07-02226.1996

Yang, J., Vitery, M. del C., Chen, J., Osei-Owusu, J., Chu, J., and Qiu, Z. (2019). Glutamate-Releasing SWELL1 Channel in Astrocytes Modulates Synaptic Transmission and Promotes Brain Damage in Stroke. *Neuron* 102, 813-827.e6. doi: 10.1016/j.neuron.2019.03.029